Bull Mar Sci. 93(2):591–609. 2017
https://doi.org/10.5343/bms.2016.1039

research paper

# Surveying the distribution and abundance of flying fishes and other epipelagics in the northern Gulf of Mexico using airborne lidar

***James H Churnside*** [1*]
***RJ David Wells*** [2]
***Kevin M Boswell*** [3]
***John A Quinlan*** [4]
***Richard D Marchbanks*** [5]
***Brandi J McCarty*** [5]
***Tracey T Sutton*** [6]

[1] *Earth System Research Laboratory, National Oceanic and Atmospheric Administration, 325 Broadway, Boulder, Colorado 80305.*

[2] *Department of Marine Biology, Texas A&M University, 1001 Texas Clipper Road, Galveston, Texas 77553.*

[3] *Department of Biological Sciences, Florida International University, 3000 NE 151st St., North Miami, Florida 33181.*

[4] *Southeast Fisheries Science Center, National Oceanic and Atmospheric Administration, 75 Virginia Beach Drive, Miami, Florida 33149.*

[5] *Cooperative Institute for Research in Environmental Sciences, University of Colorado, Boulder, Colorado 80309.*

[6] *Department of Marine and Environmental Sciences, Nova Southeastern University, 8000 N Ocean Drive, Dania Beach, Florida 33004.*

* *Corresponding author email: <james.h.churnside@noaa.gov>.*

ABSTRACT.—Flying fishes (family Exocoetidae) are important components of epipelagic ecosystems and are targeted by fishing fleets in the Caribbean Sea and elsewhere. However, owing to their anti-predator behavior and habitats, their ecology, abundance, and distributions are only partially known. From September 20 to October 6, 2011, we conducted a series of surveys over a large area (approximately 75,000 km$^2$) of the northern Gulf of Mexico (87°W–90.5°W, 28°N–30°N). The surveys used an airborne lidar and vessel-based sampling, supported by near real time satellite observations of oceanic conditions. The aerial survey was conducted from a fixed wing aircraft that flew repeated surveys day and night, enabling data collection that was both broad-scale and synoptic. Vessel-based sampling included quantitative visual observations, trawl sampling, and qualitative dip-netting for species identifications. The combined surveys identified large aggregations of epipelagic organisms dominated by flying fishes. Large numbers of jellyfish (*Aurelia* sp.) and low numbers of numerous other species were also observed. The putative flying fish aggregations had an average length scale of 6.1 km and an average population estimated at 10,000 individuals. While always near the surface, flying fish aggregations were slightly deeper at night than during the day and found most often off the continental shelf in warm water with low chlorophyll concentrations. At least three species were present: *Hirundichthys rondeletii* (Valenciennes, 1847), *Cheilopogon melanurus* (Valenciennes, 1847), and *Prognichthys occidentalis* Parin, 1999. This combination of aerial and surface surveys afforded repeated synoptic, ground-truthed data collection over a large area and indicates that this method could be useful for surveying such mobile epipelagic fishes.

Date Submitted: 1 March, 2016.
Date Accepted: 19 September, 2016.
Available Online: 29 November, 2016.

The family Exocoetidae, or flying fishes, are important components of epipelagic food webs throughout tropical and subtropical oceans. Flying fishes prey on small fishes, amphipods, mollusks, and copepods (Van Noord et al. 2013), and are prey for game fishes (Oxenford and Hunte 1999), marine mammals (Fitch and Brownell 1968), and seabirds (Tew Kai et al. 2009). They are also subject to small but important fisheries (Potts et al. 2003). However, owing to their unique predator avoidance behavior and mobility (Oxenford 1994), the abundance and spatial distribution of flying fishes (and other mobile epipelagic species) are difficult to measure directly and options for fishery-independent surveys to help manage the resource are limited. For this reason, landings reports are often used for management purposes (CRFM 2012). Landings have also been used to compare the spatial distribution of flying fishes with sea-surface temperature (SST), chlorophyll-*a* concentrations (*chl*), surface currents (Zainuddin 2011), and with meteorological conditions (Boyce 1995). While useful, such fishery-dependent data may have sampling biases, since regions of the habitat far from port will not be sampled if sufficient resources are found nearby. Thus, there remains a need to develop robust fishery-independent survey methods.

Several studies have attempted net sampling to provide information on flying fish distributions. Randall et al. (2015) quantified larval *Prognichthys occidentalis* Parin, 1999 distribution and abundance patterns relative to mesoscale features in the Gulf of Mexico using paired neuston nets in surface waters. Chang et al. (2012) collected flying fishes using gillnets during the day and dip nets with lights to attract the fish at night, but did not describe spatial distribution patterns. Casazza et al. (2005) used a towed net during the day and lights with a dip net at night to obtain specimens, also with no attempt to describe the distribution. Khokiattiwong et al. (2000) set gillnets at three depth ranges (0–1, 1–2, and 2–3 m) to demonstrate a dependence of seasonal abundance on SST, wind speed, and swell. Pitman et al. (2002) employed dip nets for flying fish and epipelagic prey and examined distribution and habitat associations via canonical correspondence analysis. Fiedler et al. (2013) used dip nets to show that the abundance of flying fish was not affected by the passage of a tropical cyclone, but their feeding success increased 3 wks after the storm.

Fewer attempts have been made to implement acoustic or tagging approaches into flying fish research. Freon (1992) attempted an acoustic survey on a towed body, but was unsuccessful. Brehmer et al. (2007) reported the first detection of flying fish aggregations by sonar, but it does not appear that this method was further developed. Studies focusing on tagging have provided general insight into movement and distribution patterns; however, it is difficult to implement on a large scale, and to examine population level abundance (Mulloney 1961, Lewis 1964, Oxenford 1994).

The most common technique for obtaining the spatial distribution of flying fishes is via visual observations of the animals as they often take flight in response to an approaching vessel. The technique was described by Breder (1929) and survey design principles were detailed by Freon (1992). This technique has been used to map the distribution of flying fishes in the Pacific Ocean (Parin 1983), where a region of high abundance was found surrounding the Eastern Equatorial Upwelling. A similar survey in the Caribbean Sea (Oxenford et al. 1995) found high abundance west of the Lesser Antilles and east of Barbados and Tobago. Khokiattiwong et al. (2000) also performed visual surveys while transiting to and from their gillnet sites, and found the highest concentrations of flying fishes 3–5.5 nmi from shore.

Here, we describe a technique for flying fish surveys using airborne lidar. There are different lidar configurations for different applications, but this application uses pulsed laser light to measure profiles of optical backscatter and depolarization along the flight track. The depth of a particular return is inferred from the two-way travel time. Fish are identified by increases in both backscatter and depolarization. This technique offers advantages over traditional methods in that it does not rely on the predator-avoidance response of the fish that may be influenced by a variety of processes, including vessel characteristics, and it can provide both large-scale synoptic coverage of large regions and high resolution surveys of areas of interest. Further, repeated synoptic surveys on effectively closed populations opens up the possibility of using Bayesian/hierarchical methods (e.g., Kéry and Royle 2016) to inform fisheries management. The basic premise of these methods is that very complicated statistical relationships among a large number of variables can be described by a hierarchy of simpler relationships using conditional statistics.

In previous work, airborne lidar has been applied to dense-schooling pelagic species including capelin [*Mallotus villosus* (Müller, 1776)] (Brown et al. 2002), Atlantic mackerel (*Scomber scombrus* Linnaeus, 1758) (Churnside et al. 2009b), Pacific sardine [*Sardinops sagax* (Jenyns, 1842)] (Churnside et al. 2009a), Pacific herring (*Clupea pallasii* Valenciennes, 1847) (Churnside et al. 2011a), Atlantic menhaden [*Brevoortia tyrannus* (Latrobe, 1802)] (Churnside et al. 2011b), and copepods (*Neocalanus* spp.) (Churnside and Thorne 2005). The present study is the first to attempt to use lidar to map less densely packed flying fish spatial distributions in the Gulf of Mexico, describe the characteristics of their aggregations, and relate their distribution to physical parameters of the upper ocean. We also highlight the need to ground-truth the aerial surveys via vessel-based sampling. Airborne surveys have been used to investigate predator-prey interactions (Churnside et al. 2011a), and could similarly be used to investigate the interactions between flying fish and zooplankton.

## Methods

### Study Area

The large (approximately 75,000 km$^2$) study area (Fig. 1) is environmentally diverse and spans water depths of 5–2500 m from near the coastline of the northern Gulf of Mexico, southward across the continental shelf, and out into the open Gulf of Mexico. The Mississippi River discharge influences water characteristics inshore, while Loop Current–associated eddies and the open Gulf of Mexico characterizes the offshore region. This region was surveyed between September 20 and October 6, 2011, to address a data gap on the distribution and abundance of epipelagic organisms in the northern Gulf of Mexico.

### Survey Design

The study was designed as a ship-supported, aerial lidar survey, which called for the aircraft to conduct broad-scale surveys across a large study area and high-resolution surveys in selected areas during the 16-d field program, weather permitting. Each daytime flight track was repeated the same night. The flight paths were arranged such that the aircraft flew over 11 stations, drawn from the Southeast Area Monitoring and Assessment Program (SEAMAP, http://www.gsmfc.org/seamap.php) standard stations (Fig. 1), within 1 d of when the ship occupied each station.

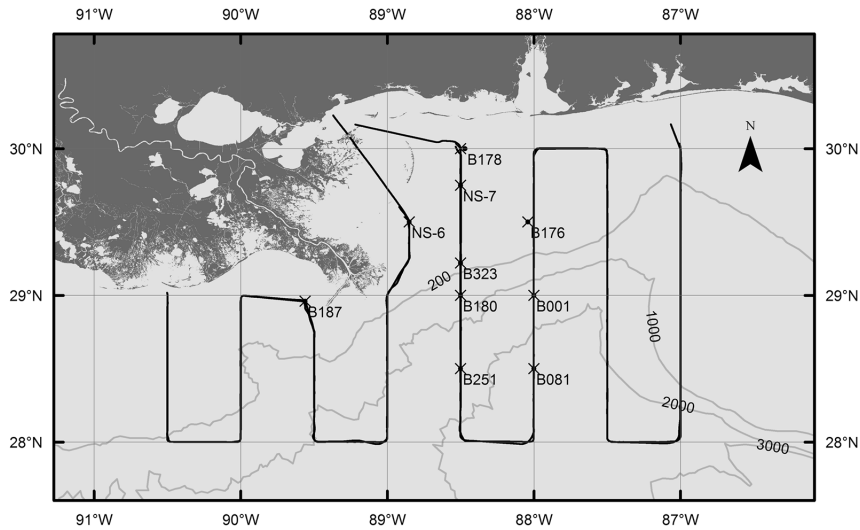


Figure 1. Chart of study area. Black lines are survey tracks for the first large-scale survey on 24-25 September, 2011, gray lines are depth contours (labeled in m), × marks the occupied ship stations labeled with the station numbers.

While the full data set was used in most of the analyses, only data near these stations were used in the comparison of aerial and surface data. The flight tracks in Figure 1 show the broad-scale pattern flown on the first 2 d of the project. Portions of this pattern were also flown near the middle of the project and at the end. In between these flights, five high-resolution surveys (i.e., a 20 × 20 km survey area with 1 nmi spacing between transect lines) were selected to study biological hotspots and frontal structures, and to include regions on the continental shelf, the slope, and over deep water. The ship engaged in both a visual survey and net sampling using a trawl and night time dip nets. Both the aircraft and the vessel were provided with daily updates on remotely sensed oceanographic conditions, and regular coordination calls took place between vessel, aircraft, and shore-side personnel.

## Shipboard Component

The vessel-based survey was conducted aboard the NOAA ship McArthur II and occupied a total of 10 stations (Fig. 1). Two of the stations were occupied twice (7 d apart) bringing the total number of shipboard data collection opportunities to 12. Generally, each opportunity included morning and evening visual counts of flying fishes, day and night trawls, and nighttime dip-net sampling.

Eleven of the vessel-based sampling opportunities were complemented by aerial coverage within 10 km of the station and within 1 d of the vessel-based data collection (i.e., the same day, the day before, or the day after), and these stations were used in the analysis presented here. Eight of the 11 vessel-based sampling opportunities were complemented by both day and night flights.

*Shipboard Visual Observations.*—Visual counts of flying fishes were secured in 10-min time observational intervals during daylight hours in the morning and evening

while transiting between sampling stations. No identification of the type of flying fish was attempted. Total visual survey time was 100 min (10, 10-min intervals) for each morning and evening survey. Four observers participated in the exercise simultaneously: two observers were stationed at the bow of the ship using small viewing quadrats (0.3 m) facing toward the direction of travel and two observers stationed on the bridge wings using large viewing quadrats (1 m) facing approximately 45° from direction of travel. Observers stood 1 m from the viewing quadrats. The counts from each observer were totaled and normalized by the quadrat size for each morning and evening survey. This was done because the effective swath width of the measurement is proportional to the quadrat size.

*Trawl Sampling.*—At each station, samples were collected with a small pelagic trawl with an opening 10 m wide by 7.5 m high, and a mesh size of 38 mm. This net was generally towed at 1 m $s^{-1}$ for 30 min during the day and at night, and sampled between the surface and an average depth of 35 m. The maximum depth sampled was 79 m. While catchability for highly mobile epipelagic organisms and densely schooling species was rather limited, the trawl collected some organisms, including fishes, scyphozoans, and crustaceans. Where possible, the total biomass per tow was measured by species. Identification of the dominant scyphozoan aggregation (*Aurelia* spp.) was by visual inspection at sea.

*Dip Net Sampling.*—Because the trawl was not effective for flying fishes, individual specimens were collected via dip-netting at night to determine the species of flying fish present at each station. This technique and the visual observations also provided information on the occurrence of other epipelagic organisms in the study area.

### Aerial Lidar Component

*Lidar Instrumentation.*—The NOAA Fisheries lidar (Churnside 2014) is a down-looking instrument that can be deployed on ships or aircraft. The light source for the lidar transmitted pulse was a frequency-doubled, Q-switched Nd:YAG laser. The laser emitted linearly-polarized, 532-nm light in 12-ns pulses at a repetition rate of 30 Hz. The laser light was directed through a polarization beam splitting cube ($10^3$ polarization extinction ratio), beam-steering mirrors, and a negative lens to ensure the light fluence at the water surface was within the American National Standards Institute (ANSI) standards for exposure to laser light (Zorn et al. 2000). The pulse energy measured after the transmission optics was 100 mJ. The lidar receiver employed two channels for measuring the returned light: one channel for the return with the same polarization as the transmitter (co-polarized return), and the other for its orthogonal polarization (cross-polarized return). For each channel, the received light was collected by a telescope, filtered by a 1-nm bandwidth interference filter, and detected by a photomultiplier tube (PMT). The 17-mrad field of view of each telescope was set to match the transmitter beam divergence. A plastic-film linear polarizer was aligned at the front of each telescope to select the appropriate linear polarization state. The photomultiplier signal was amplified through a logarithmic amplifier and digitized at 1 GHz. For the present study, the lidar system was mounted in the floor of a small twin-engine aircraft and flown at altitude of approximately 300 m over the ocean surface. The lidar system was pointed approximately 15° from nadir to minimize contribution from air-water interface reflections.

*Lidar Data Processing.*—The cross-polarized lidar return was processed by manual scrutinization similar to acoustic data processing (Churnside et al. 2011a,b). Features were identified in the lidar return and classified as either single or extended targets. Because successive pulses partially overlap, a single point in the water could be illuminated by two pulses, so a single target was defined as an enhanced return in one or two successive pulses (Fig. 2A). An enhanced return in more than two successive pulses was classified as an extended target (Fig. 2B). Single targets were typically solitary or loosely-aggregated animals, while extended targets were typically representative of densely-schooling fishes, occupying a patch diameter >5 m along the cruise track. The distinction between single and extended targets, loosely-aggregated and densely-schooling, is used later. The location, depth, and relative scattering strength of each target were recorded. Abundances (number $km^{-1}$) were calculated over 10-km long segments of flight track. For comparison with ship-based sampling data, the nearest 10-km segment to the ship was selected for each station listed in Table 1. For single targets, the 5 m swath width can be used to convert abundance into an estimate of fish density (number $km^{-2}$). This was not done for extended targets, because the effective swath depends on school size (Lo et al. 2000).

Because manually scrutinizing data is very time consuming, we investigated the performance of an automated processing technique analogous to echo integration in acoustics. An average measure of the lidar return was estimated over the same 10-km long track segments using a median-filter approach to remove background scattering effects (Carrera et al. 2006, Churnside et al. 2009a,b). The median profile of the lidar return was estimated for each 100-m section of the flight track. This profile was assumed to represent the 100-m segment's background level and was subtracted from each profile within that segment. This profile was also assumed to represent the relative attenuation and was used to normalize each profile to derive an attenuation-corrected profile, $S'(z)$, of the fish return,

$$S'(z) = \frac{[S(z) - M(z)]}{M(z)}, \qquad \text{(Eq. 1)}$$

where $S(z)$ is the original lidar profile and $M(z)$ is the median profile. To compute abundance for each section, we averaged the final value of $S'(z)$ over depth for each profile and integrated the results over the 100-m section. These values were averaged over the same 10-km segments of flight track as the manually processed values. Large changes in background scattering at scales smaller than the 100-m filter length can introduce unrealistically large values of the estimated fish return abundance. These were eliminated from the final analysis by excluding any values >3 standard deviations above the mean of all values from the same flight.

Single targets, assumed to originate from flying fishes, from the first day and night flight were separated into aggregations to assess the length scales of the flying fish aggregations. Similar approaches have been used in the past to characterize flying fish distributions (see Oxenford et al. 1995). The separation distance between sequential targets was estimated from the recorded positions. Target separations >1 km were identified, and any collection of at least 10 targets between these larger separations was considered to be an aggregation. The density of targets in an aggregation was estimated by dividing the number found in the aggregation, $N_g$, by the product of the

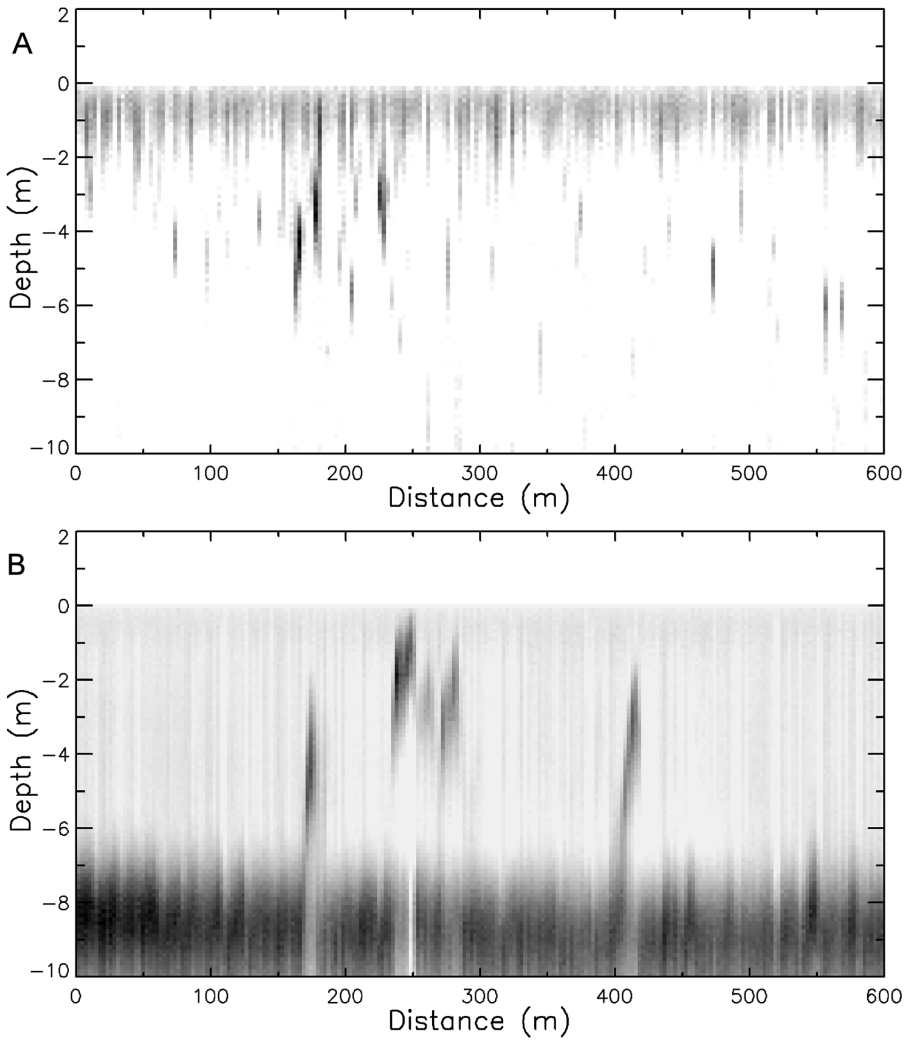


Figure 2. Lidar return as a function of depth and distance along the flight track. (A) Single targets (identified as flying fish), and (B) extended targets (identified as more tightly schooling species). The dark band at the bottom of (B) is the strong return from the sea floor.

length of the aggregation, $L_g$, and the 5-m lidar swath width. The total number in a given aggregation was then estimated as the product of the density and the area of the aggregation, which was assumed to be circular, with the result

$$N = \frac{\pi N_g L_g}{20}. \qquad \text{(Eq. 2)}$$

## Environmental Factors

The distribution and abundance of epipelagic organisms is partly determined by oceanographic conditions. To examine such associations, we used nearest-in-time Moderate-Resolution Imaging Spectroradiometer (MODIS) satellite-based estimates of chlorophyll-*a* concentration and sea-surface temperature to describe the

environment during the survey. Level 3 *chl* concentrations (4 km resolution) were secured from MODIS Aqua. Daytime and nighttime sea-surface temperatures were also obtained from MODIS (11 μ band, 4 km resolution).

### Statistical Analyses

Linear relationships between lidar targets, trawl data, and flying fish counts were assumed and we calculated the Pearson correlation coefficient with a threshold for significance of $P = 0.05$. The comparison of automated and manual lidar abundance estimates was done in the same way. For comparisons between lidar data and environmental parameters (i.e., SST, *chl*, gradients of SST and *chl*, and water depth), there was no a priori reason to suspect a linear relationship, and we calculated the Spearman correlation coefficient with the same 0.05 threshold for significance. This coefficient is appropriate when the relationship is monotonic, but not necessarily linear. To compare our results with a previous study (Zainuddin 2011), we compared the mean abundance of targets in water cooler than 27.5 °C with that in water warmer than 27.5 °C using a two-tailed Student *t*-test with the same 0.05 significance threshold. Day/night differences between lidar target aggregation characteristics were also investigated using the same test.

Because of the correlations between the environmental parameters, we also performed a principal component analysis of the environmental parameters and calculated the Spearman correlation coefficient between the lidar data and the principal components. For this analysis, the three principal components of SST, log(*chl*), and water depth were calculated. To get similar magnitudes for all three variables, we used water depth in kilometers.

We also developed a generalized additive model (GAM) for the dependence of single-target abundance and the same three environmental parameters. For this model, we smoothed the data by averaging into bins with a width of 0.1 $km^{-1}$. Using the smoothed data, we then performed a multiple linear regression of log(abundance) on depth (in km), SST, log(*chl*), and $[\log(chl)]^2$. This particular choice of model was selected from 15 variations based on a combination of simplicity and performance.

## Results

### Station Comparison

Results from the 11 vessel-based sampling opportunities complemented by aerial coverage are summarized in Table 1. The trawl samples were dominated by a scyphozoan, *Aurelia aurita* (Linnaeus, 1758), and dip nets collected three species of flying fishes: *Hirundichthys rondeletii* (Valenciennes, 1847), *Cheilopogon melanurus* (Valenciennes, 1847), and *Prognichthys occidentalis* Parin, 1999. Along with the scyphozoan, *A. aurita*, the trawl collected low numbers of other fishes, and vegetation (2.3 kg) was collected at one location (station B187). Samples with very low values for fishes (<0.01 kg per 30 min tow) were not further considered in this study and are reported as "low" in Table 1. Few individuals from densely schooling species were encountered through the trawl survey.

There were qualitative observations on the occurrence of other species not included in Table 1 that could have contributed to the lidar signal. Small numbers of herring, *Opisthonema oglinum* (Lesueur, 1818), and needlefish, *Ablennes hians* (Valenciennes, 1846), were caught in the dip nets near Station B180 on September 27,

Table 1. Summary of lidar-derived abundance estimates of extended and single targets (number of schools or individuals per km), visual counts of flying fishes, and trawl catches of the scyphozoan *Aurelia aurita* and other fishes. Values for day (first row) and night (second row) at each SEAMAP station are presented, with dashes denoting missing observations. For single targets, fish density (number per km$^2$) is abundance times 200 km$^{-1}$. If the station number is marked with an asterisk, the lidar data were part of a broad-scale survey; otherwise, they were part of a high-resolution survey. Flying fish counts have been normalized by the quadrant size (1 or 0.3 m), so the units are counts per m. Data for *Aurelia* and other fishes are total kg per tow, averaged over two tows where appropriate. Values <0.01 kg per tow are reported as low.

| Station/time | Date | Extended targets | Single targets | Flying fishes | *Aurelia* | Other fishes |
|---|---|---|---|---|---|---|
| B001* | | | | | | |
| Day | 9/23 | 0.000 | 4.800 | 5.420 | 110.00 | 0.01 |
| Night | 9/23 | 0.000 | 1.100 | — | 13.00 | 0.03 |
| B081* | | | | | | |
| Day | 9/24 | 0.000 | 11.000 | 7.750 | 0.05 | low |
| Night | 9/24 | 0.000 | 6.900 | — | 0.01 | low |
| B251 | | | | | | |
| Day | 9/25 | — | — | 25.500 | 2.20 | low |
| Night | 9/25 | — | — | — | 1.20 | low |
| B180 | | | | | | |
| Day | 9/26 | 0.000 | 0.340 | 0.404 | 12.30 | low |
| Night | 9/26 | 0.014 | 0.260 | — | 3.00 | low |
| B323 | | | | | | |
| Day | 9/28 | — | — | 0.042 | 6.80 | low |
| Night | 9/28 | — | — | — | 3.60 | low |
| NS7 | | | | | | |
| Day | 9/29 | 0.014 | 0.200 | 0.000 | 119.00 | 0.5 |
| Night | 9/29 | 0.036 | 0.100 | — | 129.00 | low |
| NS6* | | | | | | |
| Day | 9/30 | 0.000 | 0.100 | 0.100 | 72.00 | low |
| Night | 9/30 | — | — | — | 75.00 | 1.0 |
| B187* | | | | | | |
| Day | 10/1 | 0.000 | 0.000 | — | 8.40 | low |
| Night | 10/1 | 0.000 | 0.000 | — | 4.30 | 0.4 |
| B178 | | | | | | |
| Day | 10/4 | 0.036 | 0.480 | 0.000 | 20.00 | low |
| Night | 10/4 | 0.013 | 0.330 | — | 9.80 | low |
| B323 | | | | | | |
| Day | 10/5 | 0.002 | 0.120 | 8.280 | 6.80 | low |
| Night | 10/5 | 0.009 | 0.071 | — | 2.90 | low |
| NS7* | | | | | | |
| Day | 10/6 | 0.000 | 0.000 | 0.000 | 6.20 | low |
| Night | 10/6 | 0.000 | 0.000 | — | — | — |

but there was no corresponding lidar overflight. Needlefish were also caught by dip net near the same station on September 28, indicating that some of the lidar single targets in this region could be needlefish and possibly herring, though herring may be seen as extended targets (i.e., not single targets which form the core of the analyses presented here) in lidar data. Schools of blue runner, *Caranx crysos* (Mitchill, 1815), were seen near Station NS7 on September 29, but were not collected in the trawl. This is likely because they are able to swim faster than the 1 m s$^{-1}$ trawl speed.

Table 2. Summary statistics for single target detections. Mean density for all flights is reported in number of fish per square km, as are the mean density for the first flight on 24 September and the last flight on 7 October. The mean depth is of all single targets, as are the total number of aggregations identified, the fraction of all single targets found within an aggregation, the mean length of aggregations, the mean number of targets in each aggregation, and the density of targets within an aggregation in thousands of fish per square km. Uncertainty values are one standard deviation of the mean. *P* denotes significance of the day/night difference.

| | Day | Night | *P* |
|---|---|---|---|
| Mean density (fish km$^{-2}$) | 122 (SD 13) | 175 (SD 19) | 0.02 |
| Density, 24 September (fish km$^{-2}$) | 566 (SD 95) | 779 (SD 115) | 0.15 |
| Density, 7 October (fish km$^{-2}$) | 21 (SD 7) | 77 (SD 14) | <0.001 |
| Depth (m) | 4.61 (SD 0.04) | 5.27 (SD 0.04) | <0.001 |
| Number of aggregations | 125 | 90 | |
| Fraction in aggregation | 0.73 | 0.75 | |
| Mean length (km) | 3.47 (SD 0.35) | 5.18 (SD 0.67) | 0.02 |
| Aggregation size (1,000 fish) | 70 (SD 25) | 182 (SD 78) | 0.18 |
| Density (1,000 fish km$^{-2}$) | 2.19 (SD 0.14) | 2.03 (SD 0.14) | 0.43 |

Some extended lidar targets in this region could therefore be blue runner and it is interesting to note that Station NS7 did have one of the highest incidences of extended lidar targets. However, overall, very few extended targets (i.e., more densely-packed schooling organisms) were observed in the lidar near vessel-sampled stations. No significant correlations were found between total catches or scyphozoan abundance near the stations and lidar target abundance for either class (i.e., single or extended) of lidar target. However, a significant correlation was found between flying fish abundance estimated from the visual counts and single target detections near the stations ($R = 0.34$, $P = 0.014$, $n = 52$). This correlation suggests that the single targets are predominately flying fish.

### Lidar Results

Overall, the density of single target detections was slightly higher at night than during the day (Table 2). However, there was a difference between the first flight on 24 September and the last flight on 7 October. These flights are interesting, because they both covered the same tracks in the eastern portion of the large-scale survey (87°W–88.5°W). In the first flight large numbers of single targets were detected, with no day/night differences. In the last flight, relatively few single targets were detected, with a significantly larger number at night.

The lidar single target detections generally occurred in large aggregations. The individual returns in these aggregations can still be resolved, unlike the situation for extended targets, in which the returns from individuals within a school all run together in a single feature. For all flights, about 74% of single targets were within aggregations (Table 2). On the first flight, where the overall density was highest, the fraction of targets within aggregations was also highest at 91%. The distribution of the total number of targets in an aggregation was roughly lognormal (Fig. 3) with a mode near 10,000 individuals per aggregation and a good deal of variation. As expected for a lognormal distribution, the mean number was larger than the mode—117,000 overall, with no significant day/night difference (Table 3).

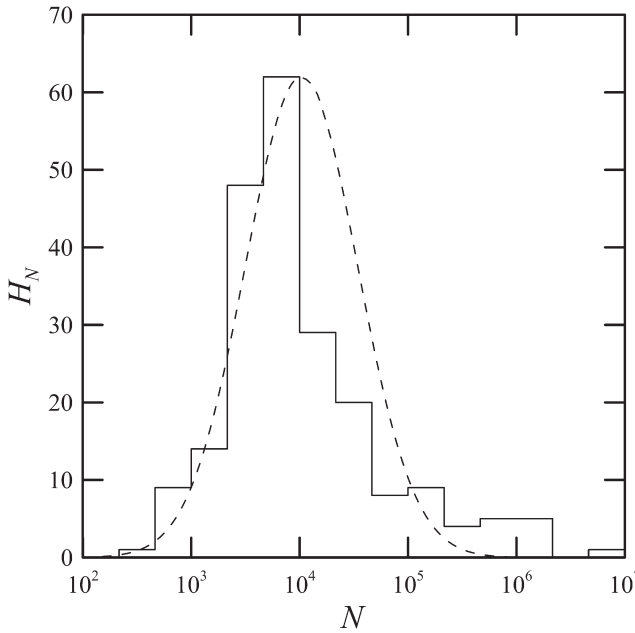


Figure 3. Histogram, $H_N$, of number of lidar targets per aggregation, $N$ (solid line), with lognormal distribution superimposed (dashed line). The lognormal distribution has the same peak value, mean logarithm, and variance of the logarithm as the data.

A comparison between the distribution of single and extended targets was conducted to see if the target classes were correlated. No significant correlation between the abundances of single and extended lidar targets was found.

The automated processing for single targets worked well when the abundances were high. Figure 4 shows the comparison of abundances for the night of 24 September. The average of the reduced lidar profiles over 10-km segments of flight track for the night of 24 September were plotted against the abundance of lidar single targets identified manually over the same segments. The Pearson correlation coefficient was 0.93, and the root-mean square difference between the data and the linear fit was 0.089.

## Environmental Dependencies

Environmental conditions in the study area ranged from the relatively cool, productive shelf water to warmer, less productive waters offshore. Significant correlations ($P < 0.001$) were observed between the lidar single-target abundances and the environmental parameters *chl* concentration, sea-surface temperature, and water

Table 3. Spearman correlation coefficients between single and extended lidar target abundances, chlorophyll-*a* concentration (*chl*), sea-surface temperature (SST), and water depth (D). There was no significant correlation between single and extended lidar target abundances. All reported correlations are significant at $P < 0.001$.

| | Single | Extended | *chl* | SST | D | PC1 | PC2 |
|---|---|---|---|---|---|---|---|
| Single | 1.00 | — | −0.37 | 0.14 | 0.40 | −0.24 | −0.33 |
| Extended | | 1.00 | 0.11 | −0.12 | −0.20 | 0.19 | — |
| *chl* | | | 1.00 | −0.37 | −0.70 | | |
| SST | | | | 1.00 | 0.37 | | |
| D | | | | | 1.00 | | |

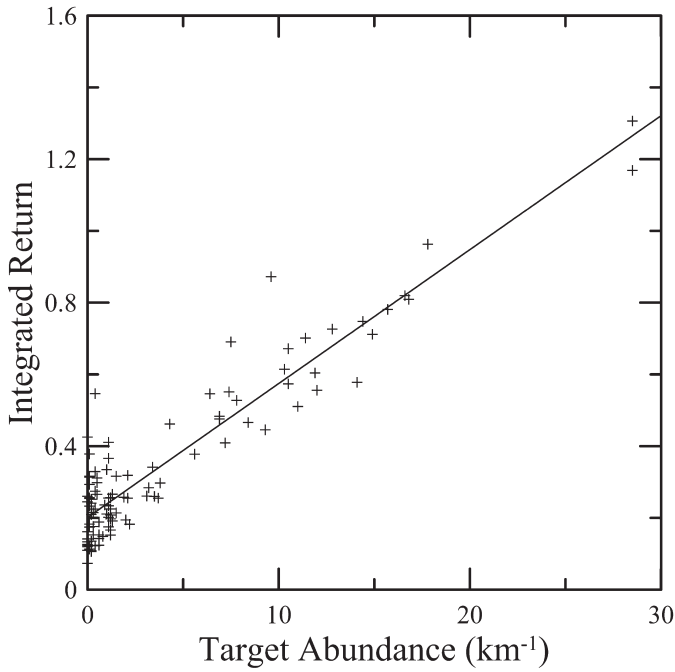


Figure 4. Integrated lidar return (uncalibrated) averaged over 10-km segments of flight track for the night of 24 September plotted against the abundance of lidar single targets identified manually over the same segments. Data (+) and the linear regression with $R^2 = 0.86$ (line) are included.

depth (Table 3). The day and night distributions of aggregations on the first large-scale survey (Fig. 5) indicated that the vast majority of the single targets (i.e., those assumed to be mostly flying fishes) were found in the southeast corner of the survey area, corresponding to warmer (SST > 27.5 °C) and less productive (*chl-a* < 1 mg $m^{-3}$) offshore waters. Most of the aggregations and the largest aggregations were found in this region (Fig. 5). The mean abundances of single targets for all flights were 0.41 (SD 0.03) $km^{-1}$ for the cooler water and 1.15 (SD 0.12) $km^{-1}$ for the warmer water, which is a statistically significant ($P < 0.0001$) difference. No difference between warm and cool water densities were found for extended targets.

The extended targets (i.e., more densely packed schools or shoals) observed by the lidar were primarily in the more productive water, while the single targets were found more often offshore. Because the relationships to environmental parameters are not necessarily expected to be linear, the Spearman correlation was calculated between the environmental parameters and the lidar target abundances for both lidar target types. These correlations are presented in Table 3 and the reported values are all significant at $P < 0.001$.

No significant correlations were found between either type of lidar target and the gradients of either sea-surface temperature or *chl* concentration. This means that we did not see a relationship between either densely packed schools or flying fish with either temperature fronts or *chl* fronts. This is the reason that the gradients were not used in the principal components analysis.

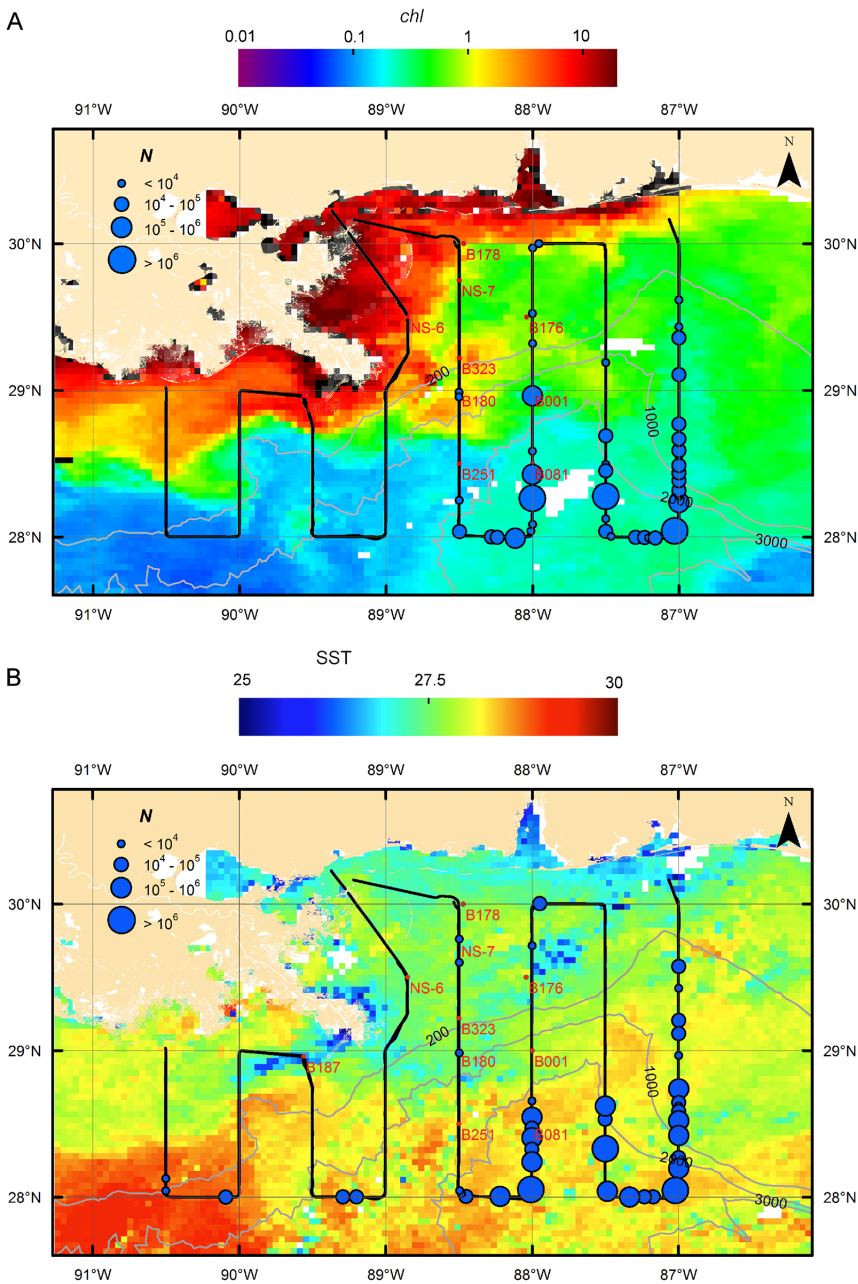


Figure 5. Number of single targets in each aggregation during the first large-scale survey. (A) daytime survey over satellite chl concentration chloraphyll (*chl*, mg $m^{-3}$), and (B) nighttime survey over satellite sea-surface temperature, SST (°C). *Chl* is a composite of the MODIS Aqua values from the OC3M algorithm over the period September 22–29, 2011. SST is a composite of the MODIS Aqua nighttime measurements at 11 μ over the period September 23–24, 2011.

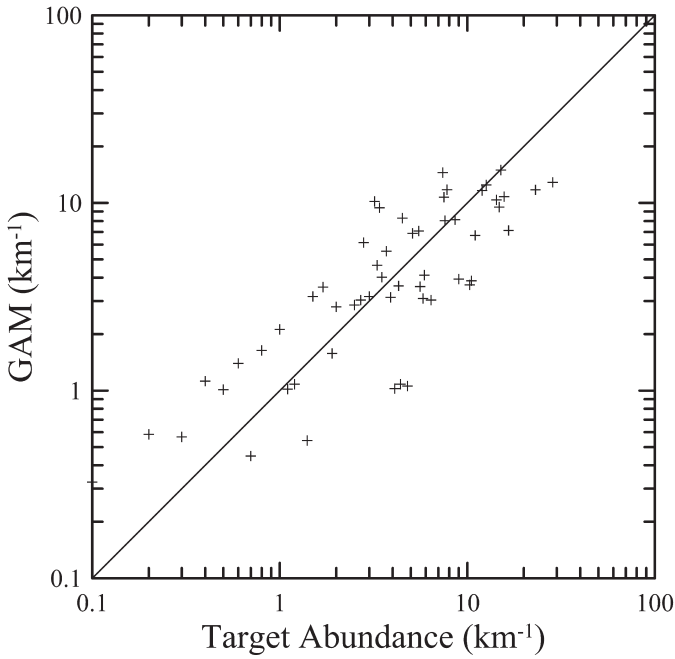


Figure 6. Prediction of the generalized additive model (GAM) as a function of the measured target abundance (+). Solid line is the expected 1:1 relationship.

The principal components were

$$\begin{aligned} PC1 &= -0.352D - 0.890\mathrm{SST} + 0.289\log(chl) \\ PC2 &= -0.798D + 0.447\mathrm{SST} + 0.404\log(chl) \\ PC3 &= 0.489 + 0.0887\mathrm{SST} + 0.868\log(chl), \end{aligned} \qquad \text{(Eq. 3)}$$

where $D$ is water depth in km. $PC1$ includes 69% of the variability and 92% is captured by the first two components. The significant correlation coefficients are listed in Table 3; extended targets were positively correlated with $PC1$ and single targets were negatively correlated with $PC1$ and $PC2$.

The GAM is given by

$$\log(\mathrm{GAM}) = -3.53 + 0.3073D + 0.0845\mathrm{SST} - 5.10\log(chl) - 4.23\log^2(chl) \qquad \text{(Eq. 4)}$$

where GAM is the model estimate for the abundance of single lidar targets. Figure 6 shows the results of Equation 4 as a function of the actual smoothed target abundance. The Pearson correlation coefficient was 0.83, and the root-mean-square error was 4.1 $km^{-1}$.

## Discussion

Surveys for mobile epipelagic organisms such as flying fishes are difficult. The most effective surveys in common use presently are either shipboard observations of flying fishes in flight (i.e., exploiting an antipredator response that could be influenced by

vessel characteristics) or gill net deployments. The use of aerial lidar to synoptically survey large areas could lead to operational surveys for these organisms. While there are uncertainties, the observed correlation between shipboard flying fish counts and lidar single target returns suggests that most, but not all, single lidar targets encountered in this field program were flying fishes. The uncertainties include issues such as catchability/detectability and patchiness that affect all sampling techniques. In future work, it might be possible to improve specificity by comparing target backscatter and depolarization with measured values for flying fish and other species. To date, these measurements have only been made for a few species (Churnside et al. 2009b, 2011b).

One challenge is patchiness in distribution that could have influenced both shipboard and lidar observations. On the afternoon of 5 October, an average abundance of 4.1 $m^{-1}$ was recorded by the two observers on the starboard side of the vessel, but the average was 27.5 $m^{-1}$ on the port side possibly indicative of patchiness in flying fish distribution. If we postulate that the lidar track missed the dense and patchy concentration of fish on the port side and remove those data from consideration, the correlation between flying fish observational counts and lidar single target numbers increases substantially (i.e., from $R = 0.34$, $P = 0.014$, $n = 52$ to $R = 0.8$, $P < 0.0001$, $n = 50$). Some of the single targets were probably needlefish, which were collected via dip net near Station 180, but the overall low numbers of single targets in this region (Fig. 5) suggest that needlefish were likely not numerous enough to greatly affect the results. The large difference between the abundances on different sides of the vessel on 5 October illustrates the large variance that occurs with limited samples sizes of organisms whose distribution is very heterogeneous. This strong dependence of the overall correlation between lidar and visual observations on this single station is consistent with a previous observation that the correlation between aerial and surface surveys was lower when the distribution of targets was less homogeneous (Carrera et al. 2006). It could be argued that, as long as ground-truthing is sufficient, the greater spatial coverage and synopticity of a lidar survey may convey advantages over purely ship-based surveys.

Another possible lidar target observed in large numbers was the scyphozoan, *A. aurita*. *Aurelia* have been detected by lidar in dense aggregations (Churnside et al. 2016), but no extended targets of this type were detected offshore even though significant numbers of *Aurelia* were collected in the trawls. The absence of a correlation between single target (i.e., not extended targets) abundance and *Aurelia* abundance as inferred from trawls suggests that *Aurelia* are not detectable by lidar at low abundance.

Two different net sampling approaches were employed: a trawl and dip nets. This survey was intended to be multispecies and collect information of epipelagic organisms. Flying fishes were able to avoid the trawl and were not collected in that gear. Nighttime dip-netting very successfully collected flying fishes, but it is not possible to use these data for quantitative abundance estimates because of the associated sampling bias. However, this sampling approach has value as it provided species composition and size data of flying fishes and also identified the presence of other mobile species, like needlefish, that could affect lidar target identification.

Some insight into the effects of misidentification of other species as flying fish can be obtained by the comparison of the first and last flights. The first flight had a large number of single target detections, with no day/night differences. The last night

had few detections, with significantly more at night. From previous tagging studies (Oxenford 1994), we know that flying fish can move up to 30 km per day, and the fish observed on the first flight could easily have moved out of the area in the 13 d until the last flight. A higher abundance of fish at night suggests the presence of vertically migrating species that are below the reach of the lidar during the day. If we use the last flight as an upper bound on the mean density of interfering species in the area, we can subtract these numbers from the overall density to get values of 101 flying fish $km^{-2}$ during the day and 98 flying fish $km^{-2}$ at night.

The average aggregation lengths of 3.5 km during the day and 5.2 km at night measured by the lidar are consistent with previous estimates of flying fish patch size. Khokiattiwong et al. (2000) reported patch sizes of 11 km or greater off Barbados. Oxenford et al. (1995) reported a mean patch size of 7.2 km in the eastern Caribbean Sea. Piontkovski and Williams (1995) reported a patch size of flying fishes of about 5 km, and pointed out that this was smaller than the patch size of the zooplankton on which they feed. To a certain extent, patch size depends on the criteria used. In one case during these surveys, for example, an aggregation 4.2-km long was separated from an aggregation 7.6 km long by a 1.6-km gap. If the criteria for distinct aggregations were separation by 2 km, rather than 1 km, these targets would all be part of a single aggregation 13.4 km long. The assumption that the aggregation length represented the diameter of a circular patch is almost certainly incorrect, but it does offer a method to scale the along-transect counts to an aerial measure. Future work with high resolution surveys may allow refinement of this metric.

The dependence of flying fishes abundance on water temperature is consistent with previous observations. For example, Zainuddin (2011) recently reported that the highest catches of flying fishes in the Flores Sea occurred in waters warmer than 27.5 °C. For the extended lidar targets, there was no significant difference in target abundance between those where the satellite SST was greater than or less than 27.5 °C. For the single lidar targets, however, the average abundance in the warmer water was about three times that in the cooler water. From a correlation alone, however, it is difficult to tell if water temperature is the determining factor in flying fish distribution. From Table 3, it is clear that SST at this time of year is positively correlated with water depth ($R = 0.37$, $P < 0.001$) and negatively correlated with *chl* concentration ($R = -0.37$, $P < 0.001$).

The distribution of fish cannot be unambiguously attributed to temperature, however. SST is positively correlated with water depth and negatively correlated with *chl* concentration, so warmer waters are also deeper and less productive. The PCA showed that most of the variability in the environment could be explained by a single component. The GAM result suggests that the dependence of abundance on the environmental parameters is not linear; the logarithm is nearly linear with water depth and SST, and quadratic with the logarithm of *chl* concentration.

The day/night depth difference in the single target data is interesting in that the targets were deeper at night than during the day (Table 2). The most likely explanation is a nocturnal change in behavior of flying fishes, perhaps driven by reduced predation pressure (i.e., fishes are not as tightly coupled to the surface layer in "flight-readiness" mode), increased focus on nocturnal zooplanktivory within the upper water column (e.g., Van Noord et al. 2013), and/or quiescence at night, with fishes slowly sinking in the water column. The latter possibility is supported by observations in the Gulf of Mexico during long nighttime conductivity-temperature-density (CTD) casts of

quiescent flying fishes with their median fins splayed (T Sutton, unpubl data), which would reduce the rate of sinking. Such behavior is rarely seen during daytime CTD casts (T Sutton, unpubl data).

Another day/night difference concerns the abundance of single targets. Near the surface vessel, this was always lower at night than during the day (Table 1). Overall, however, the average density of single targets at night was slightly higher than during the day (Table 2). One possible explanation is based on the attraction of flying fish to the ship lights at night. This might reduce the density in the region of the lidar measurements near the ship, but the data are not sufficient to test this conjecture.

No significant day/night difference was found in either the mean density of fish within the aggregations or the mean of the total number of fish estimated to be within the aggregations (Table 2). The mean length of aggregations was larger at night than during the day (Table 2), but the statistical significance of this difference barely satisfies the threshold chosen. On balance, it seems there were probably no large day/night differences in the prevalence or characteristics of the aggregations we observed.

The good agreement between the automated processing and the manually identified targets suggests that automated processing is possible for future lidar surveys of flying fishes in the Gulf of Mexico. However, this test was done using those legs of the surveys that had relatively high flying fish abundance. Additional tests under different population abundances should be performed to refine the algorithm used here.

## Conclusions

Based on the correlation with the visual observations, we conclude that airborne lidar can be a useful tool for flying fish surveys when coupled with visual observations and other groundtruthing methods from surface vessels. The aerial data provide large scale, repeated, synoptic information. The visual counts provide validation and calibration information, and dip-netting was important for species and size information. Unfortunately, and as is the case for many flying fish surveys, the vessel-based sampling faced challenges in collecting quantitative abundance data. The trawls were not successful in collecting flying fishes in the configuration used in our study and dip-netting could not be used for abundance estimation.

The lidar provided information on flying fish distribution that is difficult to obtain by other techniques. Aggregations of flying fishes were identified, with an average length of 6.1 km and an average population of 10,000 individuals. While always near the surface, flying fish aggregations were slightly deeper at night than during the day. As expected from previous work, flying fishes were found most often off of the continental shelf in warm water with low *chl* concentrations.

## Acknowledgments

This work was partially supported by the Natural Resource Damage Assessment program associated with the Deepwater Horizon event. We would like to thank the captain and crew of the R/V McArthur II and our pilots P Ramella and S Hederstedt. Satellite data were obtained from the NASA Goddard Space Flight Center, Ocean Ecology Laboratory, Ocean Biology Processing Group; (2014): MODIS-Aqua Ocean Color Data; NASA Goddard Space Flight Center, Ocean Ecology Laboratory, Ocean Biology Processing Group. http://dx.doi.org/10.5067/AQUA/MODIS_OC.2014.0. Accessed on 4 April, 2014.

## Literature Cited

Boyce SL. 1995. Sources of variability in catch per trip for flying fish (*Hirundichthys affinis*) fishery in Barbados. Cave Hill, Barbados: University of the West Indies.

Breder C. 1929. Field observations of flying fishes: a suggestion of methods. Zoologica. 9:295–312.

Brehmer P, Georgakarakos S, Josse E, Trygonis V, Dalen J. 2007. Adaptation of fisheries sonar for monitoring schools of large pelagic fish: dependence of schooling behaviour on fish finding efficiency. Aquat Living Resour. 20(4):377–384. http://dx.doi.org/10.1051/alr:2008016

Brown ED, Churnside JH, Collins RL, Veenstra T, Wilson JJ, Abnett K. 2002. Remote sensing of capelin and other biological features in the North Pacific using lidar and video technology. ICES J Mar Sci. 59(5):1120–1130. http://dx.doi.org/10.1006/jmsc.2002.1282

Carrera P, Churnside JH, Boyra G, Marques V, Scalabrin C, Uriarte A. 2006. Comparison of airborne lidar with echosounders: a case study in the coastal Atlantic waters of southern Europe. ICES J Mar Sci. 63(9):1736–1750. http://dx.doi.org/10.1016/j.icesjms.2006.07.004

Casazza TL, Ross SW, Necaise AM, Sulak KJ. 2005. Reproduction and mating behavior of the Atlantic flying fish, *Cheilopogon melanurus* (Exocoetidae), off North Carolina. Bull Mar Sci. 77(3):363–375.

Chang C, Lin C, Chen Y, Chen M, Chang S. 2012. Age validation, growth estimation and cohort dynamics of the bony flying fish *Hirundichthys oxycephalus* off eastern Taiwan. Aquat Biol. 15(3):251–260. http://dx.doi.org/10.3354/ab00425

Churnside JH. 2014. Review of profiling oceanographic lidar. Opt Eng. 53:051405. http://dx.doi.org/10.1117/1.OE.53.5.051405

Churnside JH, Brown ED, Parker-Stetter S, Horne JK, Hunt GL, Hillgruber N, Sigler MF, Vollenweider JJ. 2011a. Airborne remote sensing of a biological hot spot in the southeastern Bering Sea. Remote Sens. 3(3):621–637. http://dx.doi.org/10.3390/rs3030621

Churnside JH, Demer DA, Griffith D, Emmett RL, Brodeur RD. 2009a. Comparisons of lidar, acoustic and trawl data on two scales in the northeast Pacific Ocean. Cal Coop Ocean Fish. 50:118–122.

Churnside JH, Marchbanks RD, Donaghay PL, Sullivan JM, Graham WM, Wells RJD. 2016. Hollow aggregations of moon jellyfish (*Aurelia* spp.). J Plankton Res. 38(1):122–130. http://dx.doi.org/10.1093/plankt/fbv092

Churnside JH, Sharov AF, Richter RA. 2011b. Aerial surveys of fish in estuaries: a case study in Chesapeake Bay. ICES J Mar Sci. 68(1):239–244. http://dx.doi.org/10.1093/icesjms/fsq138

Churnside JH, Tenningen E, Wilson JJ. 2009b. Comparison of data-processing algorithms for the lidar detection of mackerel in the Norwegian Sea. ICES J Mar Sci. 66(6):1023–1028. http://dx.doi.org/10.1093/icesjms/fsp026

Churnside JH, Thorne RE. 2005. Comparison of airborne lidar measurements with 420 kHz echo-sounder measurements of zooplankton. Appl Opt. 44(26):5504–5511. http://dx.doi.org/10.1364/AO.44.005504

CRFM. 2012. Report of the First Meeting of the CRFM/WECACF Working Group on Flyingfish in the Eastern Caribbean, 18–19 June, 2012, St. Vincent and the Grenadines, CRFM Technical and Advisory Document Series Number 2012/12, Belize. 85 p.

Fiedler PC, Redfern JV, Van Noord J, Hall C, Pitman RL, Balance LT. 2013. Effects of a tropical cyclone on a pelagic ecosystem from the physical environment to top predators. Mar Ecol Prog Ser. 484:1–16. http://dx.doi.org/10.3354/meps10378

Fitch JE, Brownell RL Jr. 1968. Fish otoliths in cetacean stomachs and their importance in interpreting feeding habits. J Fish Res Board Can. 25(12):2561–2574. http://dx.doi.org/10.1139/f68-227

Freon P. 1992. A methodology for visual estimation of abundance applied to flying fish stocks. Proc Gulf Caribb Fish Inst. 41:11–35.

Kéry M, Royle JA. 2016. Applied hierarchical modeling in ecology: analysis of distribution, abundance and species richness in R and BUGS. 1st ed. Cambridge: Academic Press.

Khokiattiwong S, Mahon R, Hunte W. 2000. Seasonal abundance and reproduction of the fourwing flying fish, *Hirundichthys affinis*, off Barbados. Environ Biol Fishes. 59(1):43–60. http://dx.doi.org/10.1023/A:1007647918255

Lewis JB. 1964. Tagging experiments on the flying fish *Hirundichthys affinis* (Gunther). Bull Mar Sci Gulf Caribb. 14:381–386.

Lo NCH, Hunter JR, Churnside JH. 2000. Modeling statistical performance of an airborne lidar survey system for anchovy. Fish Bull. 98(2):264–282.

Mulloney BC. 1961. A preliminary report on the results of the tagging experiments on the flying fish *Hirundichthys affinis* (Gunther). Fish Bull. 4:1–4.

Oxenford HA. 1994. Movements of flying fish (*Hirundichthys affinis*) in the eastern Caribbean. Bull Mar Sci. 54(1):49–62.

Oxenford HA, Hunte W. 1999. Feeding habits of the dolphinfish (*Coryphaena hippurus*) in the eastern Caribbean. Sci Mar. 63(3-4):303–315. http://dx.doi.org/10.3989/scimar.1999.63n3-4317

Oxenford HA, Mahon R, Hunte W. 1995. Distribution and relative abundance of flying fish (Exocoetidae) in the eastern Caribbean: I. Adults. Mar Ecol Prog Ser. 117:11–23. http://dx.doi.org/10.3354/meps117011

Parin NV. 1983. Asessment of the abundance of flying fishes by visual observation. Biol Oceanogr. 2:341–355.

Piontkovski SA, Williams R. 1995. Multiscale variability of tropical ocean zooplankton biomass. ICES J Mar Sci. 52(3–4):643–656. http://dx.doi.org/10.1016/1054-3139(95)80078-6

Pitman RL, Ballance LT, Fiedler PC. 2002. Temporal patterns in distribution and habitat associations of prey fishes and squids. Southwest Fisheries Science Center Administrative Report LJ-02-19, available from: National Marine Fisheries Service, Southwest Fisheries Science Center, NMFS, P.O. Box 271, La Jolla, California 92038. 52 p.

Potts AC, Thomas AD, Nichols E. 2003. An economic and social assessment of the flying fish (pelagic) fishery of Tobago, Trinidad and Tobago. Proc Gulf Caribb Fish Inst. 54:635–649.

Randall LL, Smith BL, Cowan JH, Rooker JR. 2015. Habitat characteristics of bluntnose flying fish *Prognichthys occidentalis* (Actinopterygii, Exocoetidae), across mesoscale features in the Gulf of Mexico. Hydrobiologia. 749:97–111. http://dx.doi.org/10.1007/s10750-014-2151-7

Tew Kai E, Rossi V, Sudre J, Weimerskirch H Lopez C, Hernandez-Garcia E, Marsac F, Garcon V. 2009. Top marine predators track Lagrangian coherent structures. Proc Natl Acad Sci USA. 106(20):8245–8250. http://dx.doi.org/10.1073/pnas.0811034106

Van Noord JE, Lewallen EA, Pitman RL. 2013. Flying fish feeding ecology in the eastern Pacific: prey partitioning within a speciose epipelagic community. J Fish Biol. 83(2):326. http://dx.doi.org/10.1111/jfb.12173

Zainuddin M. 2011. Preliminary findings on distributions and abundance of flying fish in relation to oceanographic conditions of flores sea observed from multi-spectrum satellite images. Asian Fish Sci. 24:20–30.

Zorn HM, Churnside JH, Oliver CW. 2000. Laser safety thresholds for cetaceans and pinnipeds. Mar Mamm Sci. 16(1):186–200. http://dx.doi.org/10.1111/j.1748-7692.2000.tb00912.x